

Waves in Random and Complex Media


ISSN: (Print) (Online) Journal homepage: <https://www.tandfonline.com/loi/twrm20>

Entropy generation of magnetohydrodynamic pulsating flow of micropolar nanofluid in a porous channel through Cattaneo–Christov heat flux model with Brownian motion, thermophoresis and heat source/sink


D. Rajkumar, A. Subramanyam Reddy & Ali J. Chamkha


To cite this article: D. Rajkumar, A. Subramanyam Reddy & Ali J. Chamkha (2022): Entropy generation of magnetohydrodynamic pulsating flow of micropolar nanofluid in a porous channel through Cattaneo–Christov heat flux model with Brownian motion, thermophoresis and heat source/sink, *Waves in Random and Complex Media*, DOI: [10.1080/17455030.2022.2124467](https://doi.org/10.1080/17455030.2022.2124467)

To link to this article: <https://doi.org/10.1080/17455030.2022.2124467>

 Published online: 21 Sep 2022.

 [Submit your article to this journal](#) 

 Article views: 88

 [View related articles](#) 

 [View Crossmark data](#) 



Entropy generation of magnetohydrodynamic pulsating flow of micropolar nanofluid in a porous channel through Cattaneo–Christov heat flux model with Brownian motion, thermophoresis and heat source/sink

D. Rajkumar^a, A. Subramanyam Reddy^a and Ali J. Chamkha^b

^aDepartment of Mathematics, School of Advanced Sciences, Vellore Institute of Technology, Vellore, Tamil Nadu, India; ^bFaculty of Engineering, Kuwait College of Science and Technology, Doha District, Kuwait

ABSTRACT

The current article is to address the entropy generation on pulsating hydromagnetic flow of a micropolar nanofluid in a porous channel with the effects of Cattaneo–Christov heat flux and Buongiorno nanofluid model. This model is significant in the field of pressure surges, food processing systems, biomedical engineering, cancer therapeutic, artificial kidney, brain tumors, and nano-drug delivery in the arteries. The governing partial differential equations are converted into the system of ordinary differential equations by deploying the perturbation process then solved numerically by employing the fourth-order Runge–Kutta scheme with the support of the shooting technique. The flow variables like velocity, microrotation, temperature, nanoparticle concentration, entropy generation, and Bejan number are graphically depicted for different values of physical parameters. The heat transfer and mass transfer rates are displayed through a table. The velocity is diminishing with the enhancement of coupling parameter and Hartmann number. The temperature of nanofluid is increasing with the rising values of thermal radiation, Brownian motion, thermophoresis, and heat source while it is reduced with an enhancement of magnetic field, thermal relaxation time, and heat sink parameter. The total entropy generation is diminished by increasing the values of Hartmann number and Brownian motion.

ARTICLE HISTORY

Received 6 January 2022
Accepted 6 September 2022

KEYWORDS

Micropolar nanofluid; pulsatile flow; entropy generation; Joule heating; Hartmann number; Bejan number

Nomenclature

\tilde{x}, \tilde{y}	dimensional Cartesian coordinates
x, y	dimensionless Cartesian coordinates
\tilde{u}	dimensional velocity in the \tilde{x} direction
u	dimensionless velocity
v_0	velocity
\tilde{t}	time (s)
t	dimensionless time

CONTACT A. Subramanyam Reddy  anala.subramanyamreddy@gmail.com

P	dimensionless pressure (Pa)
B_0	strength of an applied magnetic field
h	distance between the walls
\tilde{N}	dimensional microrotation
N	dimensionless microrotation
K_1	dimensional coupling parameter
K	dimensionless coupling parameter
n	gyration parameter
P_j	micro-inertia parameter
M	Hartmann number
H	frequency parameter
q_r	radiative heat flux ($W m^{-2}$)
Ec	Eckert number
Pr	Prandtl number
Nb	Brownian motion parameter
Nt	thermophoresis parameter
Le	Lewis number
Q	heat source/sink parameter
Q_0	coefficient of heat source/sink
Rd	radiation parameter
NG	entropy generation
Be	Bejan number
\tilde{T}	temperature (K)
T_1, T_0	temperatures of top and bottom walls
\tilde{C}	fluid concentration (Moles/kg)
C_1, C_0	nanoparticles concentration of top and bottom walls
k_f	thermal conductivity ($W m^{-1} K^{-1}$)
Nu	Nusselt number
Sh	Sherwood number

Greek symbols

ε	positive quantity ($\ll 1$)
γ	chemical reaction parameter
δ	thermal relaxation time parameter
$\tilde{\sigma}$	Stefan–Boltzmann constant
η	temperature difference
ζ	temperature difference
\bar{k}	mean absorption coefficient
ρ_f	density of the fluid ($kg m^{-3}$)
ν_f	density of nanoparticles ($m^2 s^{-1}$)
$(\rho C_p)_f$	heat capacitance of the base fluid
$(\rho C_p)_s$	heat capacitance of nanoparticles
σ_f	electrical conductivity of the base fluid
θ	dimensionless temperature
θ_t	unsteady temperature

ϕ	dimensionless concentration
ϕ_t	unsteady concentration

1. Introduction

In the past two decades, nanofluids playing a vital role in heating and cooling systems. This class of fluid contains small-sized nanoparticles (100 nm) in expectable heat exchange liquids like oil, water, and ethylene glycol are called base fluids. The term 'nanofluid' was first coined by Choi [1]. The dispersion of nanoparticles in a base fluid can significantly improve heat transfer proficiency, thermal conductivity, and fluid flow properties. In recent years, many researchers and scientists had a great interest in various areas such as mechanical engineering, electronics, biomedicine, biosensors, food processes, nuclear industries, and so on [2–5]. Hence, the basic concepts of cancer treatment, chemotherapy, nanomedicine, and nano-drug delivery are also highly desirable on respective nanoparticles in chosen systems. Buongiorno [6] has developed a new approach for nanofluid flow that takes Brownian motion and thermophoresis into account. Nield and Kuznetsov [7] studied analytically for fully developed convective flow by using the Buongiorno model with the influence of thermophoresis and Brownian motion in a porous medium. Elelmy and Elgazery [8] proposed the growth of blood flow in a heart valve on a hydromagnetic non-Newtonian micropolar nanofluid with a slip effect and this model was investigated numerically. Ali et al. [9] studied MHD micropolar-based nanofluid with the Cattaneo–Christov model and bioconvective impacts by using the finite element approach. Afridi et al. [10] presented the second law of three-dimensional convective hybrid nanofluid with entropy analysis by utilizing the Runge–Kutta method fourth-order scheme. Rajput et al. [11] explored the magnetohydrodynamic flow of unsteady nonlinear nanofluid flow in a wedge by employing the Buongiorno concept. Kumar et al. [12] discussed the pulsative MHD flow of Casson nanofluid in a vertical permeable channel by considering the Buongiorno model with the effects of Ohmic heating, and thermal radiation.

Nowadays, researchers have much interest in micropolar fluids. The concept of the micropolar fluid model was first designed by Eringen [13] in 1966. The micropolar fluid is defined by rigid and arbitrarily concentrated fine particles on microrotation fluid sections. Currently, the micropolar fluid model is being gradually implemented in a variety of medical fields, and imperative applications in pharmaceutical, food industries, chemical engineering, and heat and mass transmission. Additionally, the properties of colloidal suspensions biological liquids, liquid crystals, microemulsions, polymeric blends, polymeric fluids, and exotic lubricants, respectively [14–19]. Siddiq and Ashraf [20] analyzed bioconvective micropolar nanofluid within two stretchable disks by using the Buongiorno model and the Cattaneo–Christov heat flux model. Shah et al. [21] have examined the hydromagnetic micropolar ferrofluid in a permeable channel with the effects of the Cattaneo–Christov heat flux pattern by applying the homotopy analysis method. Ahmad et al. [22] scrutinized the incompressible magnetohydrodynamic micropolar nanofluid flow in a stretching sheet with the Cattaneo–Christov heat flux model and entropy generation with slip effects. Recently, Rajkumar and Reddy [23] discussed the pulsating hydromagnetic Au/SWCNTs-blood-based micropolar nanofluid flow with the effects of viscous dissipation and heat source/sink in a porous channel.

It is well known that pulsating (or the other forms of time-changing flows such as oscillation and vibration) flow is analyzed due to a sinusoidally fluctuating pressure gradient in circular pipes/channels and is widely used in various biological aspects, medical and industrial fields around the globe. In reality, we used some applications such as control systems, the flow in hydraulic pumps, cardiovascular diseases, respiratory systems, circulatory systems, the flow ingestion or exhaust in various internal combustion engines is pulsating, the discharge of any piston pump is pulsating flow, and so on [24–30]. Abdelwahab et al. [31] considered the heat and mass transfer of pulsatile electroosmotic strength in a micropolar blood flow over intracranial aneurysms by using the finite difference method. Srinivas et al. [32] analytically studied the MHD pulsating Casson fluid flow in a permeable channel with Ohmic heating, heat source/sink, and thermal radiation by engaging the perturbation technique. Rajamani and Reddy [33] discussed the magnetohydrodynamic pulsating flow of couple stress nanofluid in a channel with Joule heating and heat source/sink by utilizing the perturbation method. Kot and Elmaboud [34] examined unsteady fractional Maxwell pulsatile blood flow in a vertical stenosed artery with a Cattaneo–Christov heat flux model.

The study of the Cattaneo–Christov heat flux model over a porous channel has a specific significance in various engineering and industrial processes. The heat transfer perceives extensive physical and technical systems including polymer extrusion, crystal budding, a portrayal of plastic films, wires, fiber, the production of paper, glass, and food [35–38]. Alebraheem and Ramzan [39] explored the heat and mass transfer of gyrotactic microorganisms through a cylinder by assuming the Cattaneo–Christov heat flux model. Jamshed et al. [40] deliberated the Williamson hybrid nanofluid with nanoparticles like copper, zirconium dioxide, and engine oil taken as base fluid by using Keller–Box’s computational method. Yahya et al. [41] elaborated the computational analysis on bioconvective and Cattaneo–Christov heat diffusion for Williamson nanofluid through the stretching surface by applying the Runge–Kutta method. The consideration of thermal radiation is a process when electromagnetic radiation is heated in all directions through a disused gap. The requirement of thermal radiation affects solar and power technology, energy transports, nuclear reactors space vehicles and satellites, and so on [42–46]. Also, the presence of a heat source/sink is essential in several fields like chemical engineering and medical reasons such as metallic sheets cooling, oil retrieval, and radial diffusers. Such an effect is supposed to be constant, space, or temperature-dependent [47–50]. Venkatesan and Reddy [51] have investigated the magnetohydrodynamic pulsatile flow with blood (base fluid) conveying Oldroyd-B base fluid and alumina as nanoparticles with the effects of heat source and thermal radiation by employing the perturbation method. Izadi et al. [52] have conducted the hydrodynamic micropolar nanofluid through the porous medium with natural convection and thermal radiation effects by utilizing the Galerkin finite element method. Abbas et al. [53] investigated the entropy analysis on hydromagnetic flow with mixed convective in a porous media by using the homotopy analysis method. Hayat et al. [54] explored the mixed convective flow by inducing the radiation effects through an inclined cylinder surface with a heat source/sink by occurring the homotopy method. Nadeem et al. [55] examined the non-Darcy porous medium with thermal radiation and heat source/sink by considering the Buongiorno model then the irreversibility process was also considered to increase the thermal energy effects.

In recent days, entropy generation is utilized in industrial sciences, engineering fields, and biological aspects. such analysis cannot work effectively due to the amount of energy generated in a thermal system and it measures the level of the existing irreversibility process. Consequently, the thermal energy performance is increased in the presence of irreversibility manner. The entropy generation depreciation in various processes like natural convection, chemical and electro-chemical, solar thermal energy, gas turbines, and air filters. Generally, Ohmic heating, viscous dissipation, and nonlinear or linear thermal radiation can be applied for entropy generation (irreversibility) in thermal progressions [56–59]. Afridi et al. [60] studied the effects on entropy generation for hydromagnetic mixed convective flow with Ohmic heating and energy dissipation by using the Sparrow–Quack–Boerner local nonsimilarity method. Almakki et al. [61] investigated the unsteady magnetohydrodynamic micropolar nanofluid with the presence of entropy generation by using the bivariate spectral quasi-linearization technique. Khan and Alzahrani [62] worked on natural convection mechanisms and mixed convective flow with entropy generation and activation energy effect. Afridi et al. [63] studied the effects of entropy production and heat transfer in a nanofluid flow in a curved surface by employing the Chebyshev–Gauss–Lobatto spectral method.

Based on the literature listed above, researchers have focused on the hydromagnetic flow of non-Newtonian nanofluid with several effects. In spite of the considerable importance of thermal radiation, Ohmic heating, and heat source/sink in various industries and engineering fields yet no study has been mentioned before which deliberate the pulsating hydromagnetic micropolar nanofluid flow with specified parameters. Therefore, the goal of this present work is to address the magnetohydrodynamic pulsating flow of a micropolar nanofluid through a porous channel with the Cattaneo–Christov heat flux concept.

- The impacts of Brownian motion, thermophoresis, chemical reaction, Ohmic heating, and viscous dissipation are examined by employing the Buongiorno model.
- In this study, we discussed the concept of entropy generation for an irreversibility process in the energy equation. At this place, blood is considered as a micropolar fluid which is signified as base fluid.
- The flow governing partial differential equations are converted into the system of ordinary differential equations by deploying the perturbation process then solved by utilizing the fourth-order Runge–Kutta procedure with the support of the shooting technique.
- The obtained numerical results have been considered for the microrotation, temperature, velocity, heat transfer rate, and Sherwood number. Finally, the motivations for involving physical parameters are discussed in detail by plotting graphs and tables.

2. Formulation of the problem

In this work, we considered a laminar and incompressible pulsatile flow of electrically treated micropolar nanofluid in a porous channel with the presence of the Cattaneo–Christov heat flux model. In this segment, the Buongiorno model is considered to analyze the Brownian motion and thermophoresis effects. The influence of Joule heating,

viscous dissipation, thermal radiation, and chemical reactions are taken into account. The delineated model of the current flow model is shown in Figure 1. A Cartesian coordinate process is used to examine the flow such that the \tilde{x} -axis is along with the bottom wall and the \tilde{y} -axis is perpendicular to the walls. The fluid is supposed to shoot into the channel, which is located at $\tilde{y} = 0$ with velocity v_0 and is squeezed out with unvaried velocity v_0 over the top wall at $\tilde{y} = h$.

An applied magnetic field B_0 is imposed consistently normal to both the walls. The induced magnetic field is neglected. T_1 and T_0 are temperatures at the top and bottom walls accordingly ($T_0 < T_1$), C_1 and C_0 are the nanoparticle concentrations of top and bottom walls respectively ($C_0 < C_1$). Under these hypotheses, the governing equations are given by [12, 25, 28, 32]

$$\frac{\partial \tilde{u}}{\partial \tilde{t}} + v_0 \frac{\partial \tilde{u}}{\partial \tilde{y}} = -\frac{1}{\rho_f} \frac{\partial \tilde{P}}{\partial \tilde{x}} + \left(\frac{\mu_f + K_1}{\rho_f} \right) \frac{\partial^2 \tilde{u}}{\partial \tilde{y}^2} - \frac{\sigma_f B_0^2}{\rho_f} \tilde{u} + \frac{K_1}{\rho_f} \frac{\partial \tilde{N}}{\partial \tilde{y}}, \quad (1)$$

$$\frac{\partial \tilde{N}}{\partial \tilde{t}} + v_0 \frac{\partial \tilde{N}}{\partial \tilde{y}} = -\frac{1}{\rho_{fj}} 2K_1 \tilde{N} - \frac{K_1}{\rho_{fj}} \frac{\partial \tilde{u}}{\partial \tilde{y}} + \frac{\gamma}{\rho_{fj}} \frac{\partial^2 \tilde{N}}{\partial \tilde{y}^2}, \quad (2)$$

$$\begin{aligned} \frac{\partial \tilde{T}}{\partial \tilde{t}} + v_0 \frac{\partial \tilde{T}}{\partial \tilde{y}} + \lambda_2 \left(\frac{\partial^2 \tilde{T}}{\partial \tilde{t}^2} + v_0^2 \frac{\partial^2 \tilde{T}}{\partial \tilde{y}^2} + 2v_0 \frac{\partial^2 \tilde{T}}{\partial \tilde{y} \partial \tilde{t}} \right) \\ = \frac{k_f}{(\rho C_p)_f} \frac{\partial^2 \tilde{T}}{\partial \tilde{y}^2} + \tau \left[D_B \left(\frac{\partial \tilde{C}}{\partial \tilde{y}} \frac{\partial \tilde{T}}{\partial \tilde{y}} \right) + \frac{D_T}{T_m} \left(\frac{\partial \tilde{T}}{\partial \tilde{y}} \right)^2 \right] + \frac{\mu_f + K_1}{(\rho C_p)_f} \left(\frac{\partial \tilde{u}}{\partial \tilde{y}} \right)^2 \\ + \frac{\sigma_f B_0^2}{(\rho C_p)_f} \tilde{u}^2 - \frac{1}{(\rho C_p)_f} \frac{\partial q_r}{\partial \tilde{y}} + \frac{Q_0}{(\rho C_p)_f} (\tilde{T} - T_0), \end{aligned} \quad (3)$$

$$\frac{\partial \tilde{C}}{\partial \tilde{t}} + v_0 \frac{\partial \tilde{C}}{\partial \tilde{y}} = D_B \frac{\partial^2 \tilde{C}}{\partial \tilde{y}^2} + \frac{D_T}{T_m} \frac{\partial^2 \tilde{T}}{\partial \tilde{y}^2} - k_r \tilde{C}, \quad (4)$$

where \tilde{u} is the velocity component along with the \tilde{x} -direction, k_f , σ_f , μ_f , ρ_f , and $(\rho C_p)_f$ represent thermal conductivity, electrical conductivity, dynamic viscosity, density, and effective specific heat of nanofluid, respectively. \tilde{P} is the fluid pressure, \tilde{T} and \tilde{C} are the dimensional temperature and concentration of the nanofluid, j is the micro-inertia parameter, \tilde{N} is the microrotation vector, q_r is the radiative heat flux, K_1 is the coupling parameter, λ_1 is the

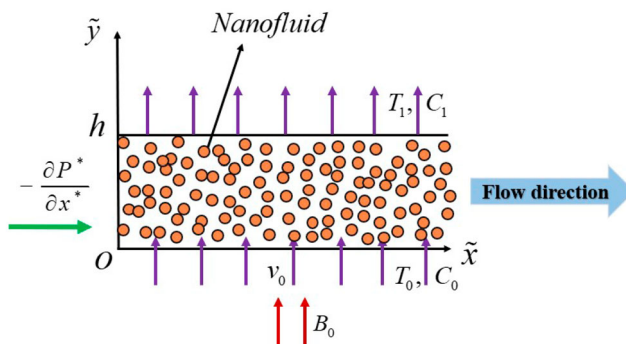


Figure 1. Flow geometry.

thermal relaxation time parameter, $(\rho C_p)_p$ is the effective heat capacity of the nanoparticles accordingly, $\tau = (\rho C_p)_p / (\rho C_p)_f$, k_f , T_m , D_B , and D_T are the first-order chemical reaction rate, mean temperature, Brownian diffusion coefficient, and the thermophoretic diffusion, respectively.

The corresponding boundary conditions (BCs) are

$$\tilde{u} = 0, \quad \tilde{N} = 0, \quad \tilde{T} = T_0, \quad \tilde{C} = C_0 \quad \text{at } \tilde{y} = 0, \quad (5)$$

$$\tilde{u} = 0, \quad \tilde{N} = 0, \quad \tilde{T} = T_1, \quad \tilde{C} = C_1 \quad \text{at } \tilde{y} = h. \quad (6)$$

Here h is the distance between the walls.

Now, by using the Rosseland approximation to the radiative heat flux model q_r , Equation (3) becomes

$$\begin{aligned} \frac{\partial \tilde{T}}{\partial \tilde{t}} + v_0 \frac{\partial \tilde{T}}{\partial \tilde{y}} + \lambda_2 \left(\frac{\partial^2 \tilde{T}}{\partial \tilde{u}^2} + v_0^2 \frac{\partial^2 \tilde{T}}{\partial \tilde{y}^2} + 2v_0 \frac{\partial^2 \tilde{T}}{\partial \tilde{y} \partial \tilde{t}} \right) \\ = \frac{k_f}{(\rho C_p)_f} \frac{\partial^2 \tilde{T}}{\partial \tilde{y}^2} + \tau \left[D_B \left(\frac{\partial \tilde{C}}{\partial \tilde{y}} \frac{\partial \tilde{T}}{\partial \tilde{y}} \right) + \frac{D_T}{T_m} \left(\frac{\partial \tilde{T}}{\partial \tilde{y}} \right)^2 \right] + \frac{\mu_f + K_1}{(\rho C_p)_f} \left(\frac{\partial \tilde{u}}{\partial \tilde{y}} \right)^2 \\ + \frac{\sigma_f B_0^2}{(\rho C_p)_f} \tilde{u}^2 + \frac{1}{(\rho C_p)_f} \frac{16\sigma^* T_0^3}{3\tilde{k}} \frac{\partial^2 \tilde{T}}{\partial \tilde{y}^2} + \frac{Q_0}{(\rho C_p)_f} (\tilde{T} - T_0), \end{aligned} \quad (7)$$

where $\tilde{\sigma}$ is the Stefan–Boltzmann constant and \tilde{k} is the mean absorption coefficient.

By utilization of the succeeding dimensionless parameters,

$$\left. \begin{aligned} x = \frac{\tilde{x}}{h}, \quad y = \frac{\tilde{y}}{h}, \quad N = \frac{\tilde{N}h}{v_0}, \quad u = \frac{\tilde{u}}{v_0}, \quad t = \omega \tilde{t}, \\ P = \frac{\tilde{P}h}{\mu_f v_0}, \quad \theta = \frac{\tilde{T} - T_0}{T_1 - T_0}, \quad \phi = \frac{\tilde{C} - C_0}{C_1 - C_0}. \end{aligned} \right\} \quad (8)$$

By using dimensionless parameters Equations (1), (2), (4), and (7) turn as

$$H^2 \frac{\partial u}{\partial t} + R \frac{\partial u}{\partial y} = -\frac{\partial P}{\partial x} + (1 + K) \frac{\partial^2 u}{\partial y^2} - M^2 \tilde{u} + K \frac{\partial N}{\partial y}, \quad (9)$$

$$P_j H^2 \frac{\partial N}{\partial t} + R \frac{\partial N}{\partial y} = -2nN - n \frac{\partial u}{\partial y} + \frac{\partial^2 N}{\partial y^2}, \quad (10)$$

$$\begin{aligned} H^2 \frac{\partial \theta}{\partial t} + R \frac{\partial \theta}{\partial y} + \delta \left(H^2 \frac{\partial^2 \theta}{\partial t^2} + \frac{R^2}{H^2} \frac{\partial^2 \theta}{\partial y^2} + 2R \frac{\partial^2 \theta}{\partial y \partial t} \right) \\ = \frac{1}{Pr} \left(1 + \frac{4}{3} Rd \right) \frac{\partial^2 \theta}{\partial y^2} + (1 + K) Ec \left(\frac{\partial u}{\partial y} \right)^2 + Ec M^2 u^2 \\ + Nb \frac{\partial \theta}{\partial y} \frac{\partial \phi}{\partial y} + Nt \left(\frac{\partial \theta}{\partial y} \right)^2 + Q\theta, \end{aligned} \quad (11)$$

$$LePrH^2 \frac{\partial \phi}{\partial t} + RPrLe \frac{\partial \phi}{\partial y} = \frac{\partial^2 \phi}{\partial y^2} + \frac{Nt}{Nb} \frac{\partial^2 \theta}{\partial y^2} - \gamma LePr\phi - K_c LePr, \quad (12)$$

where v_0 is the velocity, ω is the frequency, $K = \frac{K_1}{\mu_f}$ is the coupling parameter, $Ec = \frac{v_0^2}{(C_p)_f (T_1 - T_0)}$ is the Eckert number, $M = B_0 h \sqrt{\frac{\sigma_f}{\mu_f}}$ is the Hartmann number, $n = \frac{K_1 h^2}{\gamma}$ is the

gyration parameter, $P_j = \frac{j\mu_f}{\gamma}$ is the micro-inertia parameter, $H = \frac{h\sqrt{\omega}}{\sqrt{\nu_f}}$ is the frequency parameter, $Nb = \frac{\tau D_B(C_1 - C_0)}{\nu_f}$ is the Brownian motion parameter, $Nt = \frac{\tau D_T(T_1 - T_0)}{T_m \nu_f}$ is the thermophoresis, $\delta = \omega \lambda_2$ is the thermal relaxation time parameter, $Pr = \frac{\nu_f}{\alpha_1}$ is the Prandtl number, $Le = \frac{\alpha_1}{D_B}$ is the Lewis number, $Rd = \frac{4\sigma T_0^3}{k_f k}$ is the radiation parameter, $\gamma = \frac{k_f h^2}{\nu_f}$ is the chemical reaction parameter, $K_c = \frac{k_f C_0 h^2}{\nu_f (C_1 - C_0)}$.

The appropriate BCs are

$$\text{At } y = 0 \Rightarrow u = 0, \quad N = 0, \quad \theta = 0, \quad \phi = 0, \quad (13)$$

$$\text{At } y = 1 \Rightarrow u = 0, \quad N = 0, \quad \theta = 1, \quad \phi = 1. \quad (14)$$

3. Solution of the problem

The pressure gradient of the form is supposed to stimulate the pulsating flow follows as [17]

$$-\frac{\partial P}{\partial x} = \lambda_0 + \varepsilon \lambda_1 e^{it}. \quad (15)$$

Since, the pressure gradient causes the pulsatile flow given in Equation (15), the velocity, microrotation, temperature, and nanoparticle concentration are taken as

$$u = u_0(y) + \varepsilon u_1(y)e^{it}, \quad (16)$$

$$N = N_0(y) + \varepsilon N_1(y)e^{it}, \quad (17)$$

$$\theta = \theta_0(y) + \varepsilon \theta_1(y)e^{it}, \quad (18)$$

$$\phi = \phi_0(y) + \varepsilon \phi_1(y)e^{it}. \quad (19)$$

Substituting Equations (15)–(19) in Equations (9)–(12) and matching the power of ε , we obtain

$$(1 + K)u_0'' - R(u_0') - M^2(u_0) + K(N_0') + \lambda_0 = 0, \quad (20)$$

$$(1 + K)u_1'' - R(u_1') - (M^2 + H^2 i)u_1 + K(N_1') + \lambda_1 = 0, \quad (21)$$

$$N_0'' - P_j R(N_0') - 2n(N_0) - n(u_0') = 0, \quad (22)$$

$$N_1'' - P_j R(N_1') - (2n + iH^2 P_j)N_1 - n(u_1') = 0, \quad (23)$$

$$\frac{1}{Pr} \left(1 + \frac{4}{3}Rd - \delta \frac{R^2}{H^2} \right) \theta_0'' - R\theta_0' + Nb(\theta_0'\phi_0') + Nt(\theta_0')^2 + Q\theta_0 + (1 + K)Ec(u_0')^2 + M^2 Ec(u_0)^2 = 0, \quad (24)$$

$$\frac{1}{Pr} \left(1 + \frac{4}{3}Rd - \delta \frac{R^2}{H^2} \right) \theta_1'' - R\theta_1' - 2\delta R\theta_1' - iH^2\theta_1 - \delta H^2 i^2 \theta_1 + Nb(\theta_1'\phi_0' + \theta_0'\phi_1') + 2Nt(\theta_1'\theta_0') - iH^2\theta_1 + 2(1 + K)Ec(u_1' u_0') + 2M^2 Ec(u_0 u_1) = 0, \quad (25)$$

$$\phi_0'' - RLePr(\phi_0') - \gamma LePr(\phi_0) + \frac{Nt}{Nb}(\theta_0'') - K_c LePr = 0, \quad (26)$$

$$\phi_1'' - RLePr(\phi_1') - LePr(\gamma + H^2 i)\phi_1 + \frac{Nt}{Nb}(\theta_1'') = 0. \quad (27)$$

The corresponding BCs are

$$\left. \begin{aligned} \text{At } y = 0 &\Rightarrow u_0 = 0, \quad N_0 = 0, \quad \theta_0 = 0, \quad \phi_0 = 0, \quad u_0 = 0, \quad N_0 = 0, \quad \theta_0 = 0, \quad \phi_0 = 0, \\ \text{At } y = 1 &\Rightarrow u_0 = 0, \quad N_0 = 0, \quad \theta_0 = 1, \quad \phi_0 = 1, \quad u_1 = 0, \quad N_1 = 0, \quad \theta_1 = 0, \quad \phi_1 = 0. \end{aligned} \right\} \quad (28)$$

Furthermore, the nondimensional heat transfer rate (Nusselt number) and rate of mass transfer (Sherwood number) at the walls are assigned as

$$Nu = (\theta'_0(y) + \varepsilon\theta'_1(y)e^{it})_{y=0,1}, \quad (29)$$

$$Sh = (\phi'_0(y) + \varepsilon\phi'_1(y)e^{it})_{y=0,1}. \quad (30)$$

The system of nonlinear ODEs (20)–(27) with the BCs (28) are solved numerically by adopting the Runge–Kutta fourth-order method along with the shooting approach. The step size is fixed as 0.001 (i.e. $\Delta y = 0.001$) and precision is static for the convergence standards. To the best of the authors knowledge, no experimental work has been carried out in this direction. To check the correctness of the present results we made a comparison between the present results and the results obtained by NDSolve using MATHEMATICA software which are given in Table 1. It is observed that there is a good agreement between the present results and the results obtained by NDSolve.

3.1. Analysis of entropy generation

$$\begin{aligned} Ns = & \frac{K_f}{T_0^2} \left[1 + \frac{16\tilde{\sigma}T_0^3}{3\tilde{k}k_f} \right] \left(\frac{\partial \tilde{T}}{\partial \tilde{y}} \right)^2 + \frac{\mu_f + K_1}{T_0} \left(\frac{\partial \tilde{u}}{\partial \tilde{y}} \right)^2 + \frac{\sigma_f B_0^2 \tilde{u}^2}{T_0} \\ & + \frac{R_D}{C_0} \left(\frac{\partial \tilde{C}}{\partial \tilde{y}} \right)^2 + \frac{R_D}{T_0} \frac{\partial \tilde{T}}{\partial \tilde{y}} \frac{\partial \tilde{C}}{\partial \tilde{y}}. \end{aligned} \quad (31)$$

Table 1. Comparison between the present results and the results obtained by NDSolve for $\theta'(0)$ when $\varepsilon = 0.1$, $t = \frac{\pi}{4}$, $Ec = 0.5$, $Pr = 21$, $K = 0.5$, $H = 2$, $Rd = 1$, $Q = 0.5$, $R = 1$, $\delta = 0.1$, $P_j = 1$, $M = 1$, $Nb = 0.1$, $Nt = 0.1$, $Kr = 0.001$, $Le = 1$, $\gamma = 1$, $\lambda_0 = 1$, and $\lambda_1 = 1$.

Parameter	Values	Present results	NDSolve
		$\theta'(0)$	$\theta'(0)$
Rd	1	0.07656730	0.07656747
	2	0.14534063	0.14534063
	3	0.25578567	0.25578568
M	1	0.07656730	0.07656747
	2	0.05559120	0.05559126
	3	0.03861895	0.03861898
Nb	0.23	0.07941498	0.07941420
	0.26	0.08278743	0.08278773
	0.30	0.08826149	0.08826196
Nt	0.23	0.08058313	0.08058357
	0.26	0.08574748	0.08574856
	0.30	0.09512609	0.09512946

The nondimensional form of entropy generation rate is

$$NG = \left(1 + \frac{4Rd}{3}\right) \left(\frac{\partial\theta}{\partial y}\right)^2 + \frac{M^2 EcPr}{\eta} u^2 + \left(\frac{(1+K)EcPr}{\eta}\right) \left(\frac{\partial u}{\partial y}\right)^2 + \frac{\lambda\zeta}{\eta^2} \left(\frac{\partial\phi}{\partial y}\right)^2 + \frac{\lambda}{\eta} \frac{\partial\theta}{\partial y} \frac{\partial\phi}{\partial y}, \quad (32)$$

where $\eta = \frac{T_1 - T_0}{T_0}$ is the temperature difference, $\lambda = \frac{R_D(C_1 - C_0)}{k_f}$ is the diffusivity, R is the gas constant, D is the diffusion, $\zeta = \frac{C_1 - C_0}{C_0}$ is the concentration difference

$$NG = NG_0(y) + \varepsilon NG_1(y)e^{it}, \quad (33)$$

Now by substituting Equations (16), (18), (19), and (33) into Equation (32), and considering the coefficients power of ε , one can get

$$NG_0 = \left(1 + \frac{4Rd}{3}\right) (\theta'_0)^2 + \frac{M^2 EcPr}{\eta} u_0^2 + \frac{(1+K)EcPr}{\eta} (u'_0)^2 + \left(\frac{\lambda\zeta}{\eta^2}\right) \phi_0'^2 + \left(\frac{\lambda}{\eta}\right) \theta'_0 \phi'_0, \quad (34)$$

$$NG_1 = 2 \left(1 + \frac{4Rd}{3}\right) \theta'_0 \theta'_1 + \frac{2M^2 EcPr}{\eta} u_0 u_1 + \frac{2EcPr(1+K)}{\eta} u'_0 u'_1 + \left(\frac{2\lambda\zeta}{\eta^2}\right) \phi'_0 \phi'_1 + \left(\frac{\lambda}{\eta}\right) (\phi'_0 \theta'_1 + \phi'_1 \theta'_0), \quad (35)$$

$$\text{Bejan number(Be)} = \frac{\text{Heat and mass transfer irreversibility}}{\text{Total entropy generation}}$$

$$\text{Be} = \frac{\left(1 + \frac{4Rd}{3}\right) \left(\frac{\partial\theta}{\partial y}\right)^2 + \left(\frac{\lambda\zeta}{\eta^2}\right) \left(\frac{\partial\phi}{\partial y}\right)^2 + \left(\frac{\lambda}{\eta}\right) \frac{\partial\theta}{\partial y} \frac{\partial\phi}{\partial y}}{NG}. \quad (36)$$

4. Results and discussion

In this section, the impacts of different parameters on velocity, microrotation, temperature, and entropy generation are presented graphically in terms of Figures 2–11. The heat and mass transfer rates are illustrated in Table 2. For simulation reasons, the standard values adjusted at $M = 1, Rd = 1, H = 2, Q = 0.5, K = 1, Ec = 0.5, \delta = 0.1, \zeta = 1, \lambda = 1, Nb = 0.2, Nt = 0.2, Pr = 21, P_j = 1, \lambda_0 = 1, \lambda_1 = 1, \gamma = 1, Le = 0.5, \eta = 1, \varepsilon = 0.001$, and $t = \pi/4$. The deviations of the steady velocity (u_0) for various parameters such as coupling parameter (K), Hartmann number (M), gyration parameter (n), and cross-flow Reynolds number (R) are shown in Figure 2(a–d). Figure 2(a) depicts the variations in the steady velocity for giving higher values of coupling parameter. This is due to the coupling parameter opposing the flow then the steady velocity behavior is degrading and it leads to decreasing velocity. Figure 2(b) depicts that the steady velocity is decelerating with an increment of Hartmann number. The reason behind this is Lorentz forces which are generated by the applied magnetic field acting in the perpendicular path to the flow direction of the micropolar nanofluid. Hence, there is a reduction in steady velocity. Figure 2(c) reveals that the steady velocity is

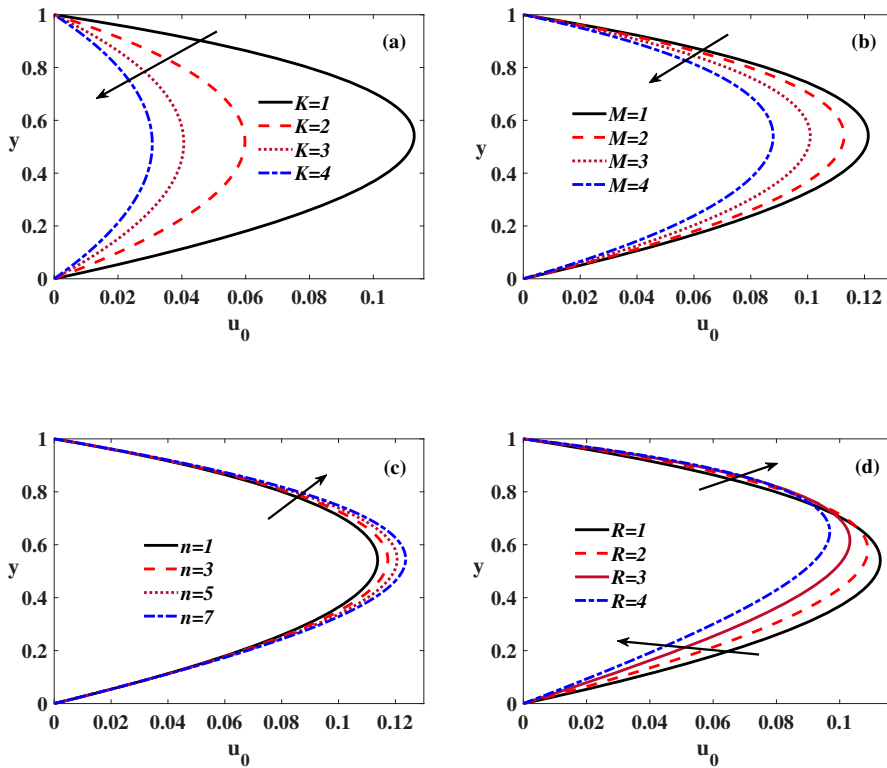


Figure 2. (a) Impact of K on u_0 . (b) Impact of M on u_0 . (c) Impact of n on u_0 . (d) Impact of R on u_0 .

augmented when giving higher values of gyration parameter. This is due to the fluid quantities, which have been related to the shear stress by the micro-gyration vector. Figure 2(d) shows that the steady velocity is diminished near to the injection wall (lower wall) with the increment of cross-flow Reynolds number although they are upsurged close to the suction wall (upper wall).

The variations of unsteady velocity (u_t) of several parameters such as cross-flow Reynolds number (R), Hartmann number (K), gyration parameter (n), coupling parameter (K), and time (t) are displayed in Figure 3(a–e). Figure 3(a) shows the differences in the unsteady velocity for giving the higher values of coupling parameter. This is due to the coupling parameter opposing the flow, which induces the unsteady velocity behavior to diminish, causing the velocity to decrease. The same behavior represents the improvement in Hartmann number as shown in Figure 3(b). Because of Lorentz forces, which have been produced by an applied magnetic field acting perpendicular to the flow direction. As a result, velocity decreases. Figure 3(c) shows that the unsteady velocity of the micropolar nanofluid is diminished due to increasing the values of gyration parameter. Figure 3(d) shows that the unsteady velocity is reduced near the injection wall (bottom wall) with the increment of cross-flow Reynolds number at the same time they are enhanced close to the squeezed wall (top wall). Figure 3(e) exhibits that the unsteady velocity oscillates with rising time (t).

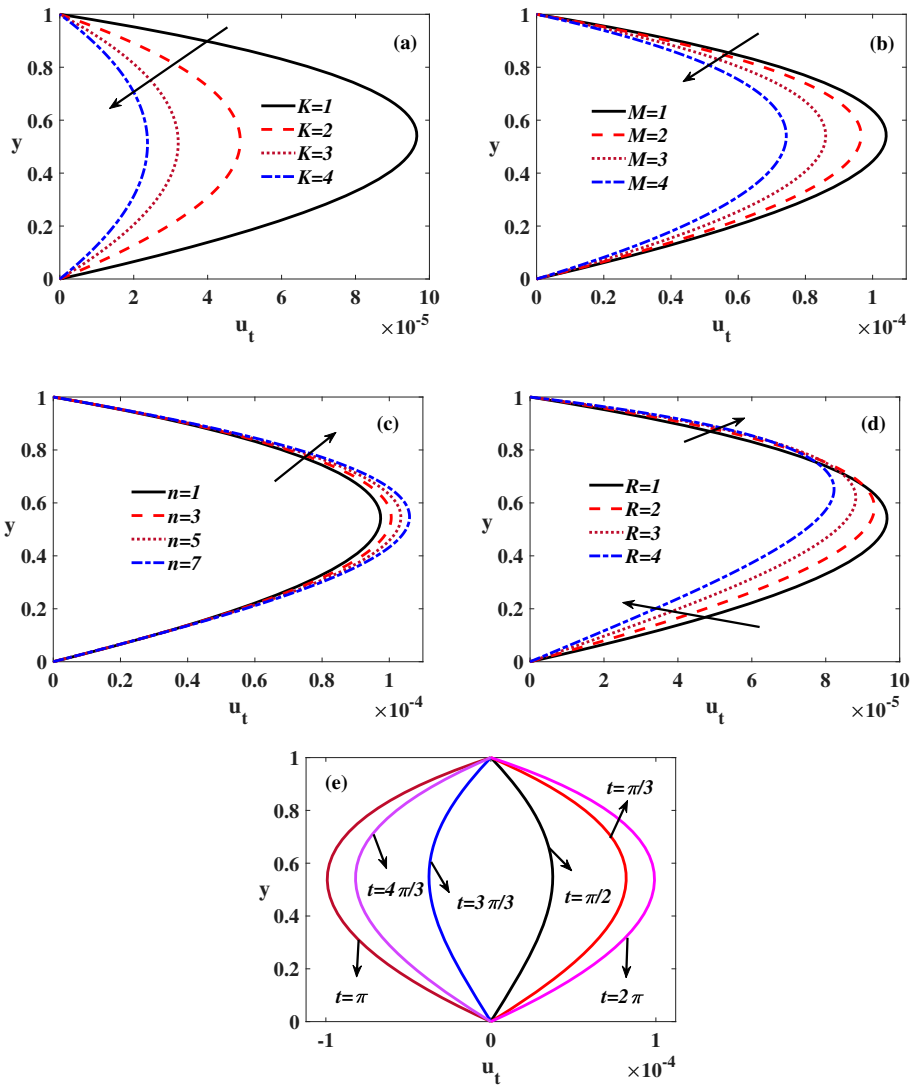


Figure 3. (a) Impact of K on u_t . (b) Impact of M on u_t . (c) Impact of n on u_t . (d) Impact of R on u_t . (e) Impact of t on u_t .

The profiles of steady microrotation (N_0) are presented by considering the coupling parameter, micro-inertia parameter (P_j), gyration parameter (n), and Hartmann number (M) in Figure 4(a–d). Figure 4(a) demonstrates that the steady microrotation is falling close to the upper wall and rising near to the lower wall for escalating values of coupling parameter. Because the coupling parameter opposes the movement and thus induces the steady microrotation. Figure 4(b) describes that the steady microrotation is upsurged near to top wall and reduced near the bottom wall by enhancing the Hartmann number. Because Lorentz forces are created by the utilized magnetic field acting in the perpendicular way to the flow direction. Figure 4(c) describes that the steady microrotation is turned up near

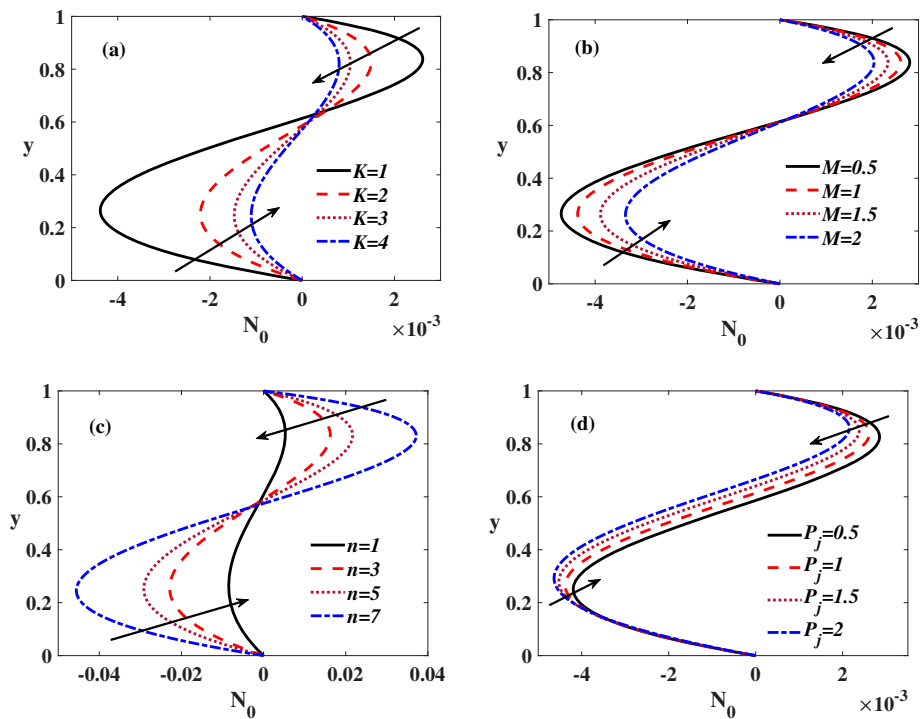


Figure 4. (a) Impact of K on N_0 . (b) Impact of M on N_0 . (c) Impact of n on N_0 . (d) Impact of P_j on N_0 .

the top wall and turns down near the bottom wall by accelerating in the gyration parameter. This is due to the fluid quantities which are a relationship between the micro-gyration vector to the shear stress. Figure 4(d) displays that the steady microrotation is diminishing near to the upper wall and rising near to the lower wall by giving higher values of micro-inertia parameter. The reason is micropolar fluids that are able to support stress moments with body couples and are influenced by spin inertia.

Figure 5(a–e) shows the variances of the unsteady microrotation (N_t) for coupling parameter (K), Hartmann number (M), gyration parameter (n), micro-inertia parameter (P_j), and time (t). Figure 5(a) depicts that the unsteady microrotation is dropping nearby the upper wall and mounting nearby the lower wall for rising values of coupling parameter. This is because the coupling parameter opposes the flow, allowing the unsteady microrotation to oscillate. Figure 5(b) exhibits that the unsteady microrotation is bringing down close to the upper wall and the bottom wall brings up with increasing values of Hartmann number. Figure 5(c) shows that the unsteady microrotation is moved up in the top wall and it moves down near to the bottom wall. This is due to the micro-gyration vector being related to the shear stress when fluid is quantified and it causes to fluctuate in the fluid flow. The opposite behavior occurs due to giving the higher values in the micro-inertia parameter which is shown in Figure 5(d). Figure 5(e) designates that the unsteady microrotation is wavering near to both the walls by varying values in time.

The influences of Ec , M , δ , Nb , Q , Rd , and Nt for steady temperature (θ_0) are exhibited in Figure 6(a–g). Figure 6(a) reveals that the steady temperature is upsurged by enhancing the Eckert number (Ec). Because viscous dissipation is related to heat enthalpy and kinetic

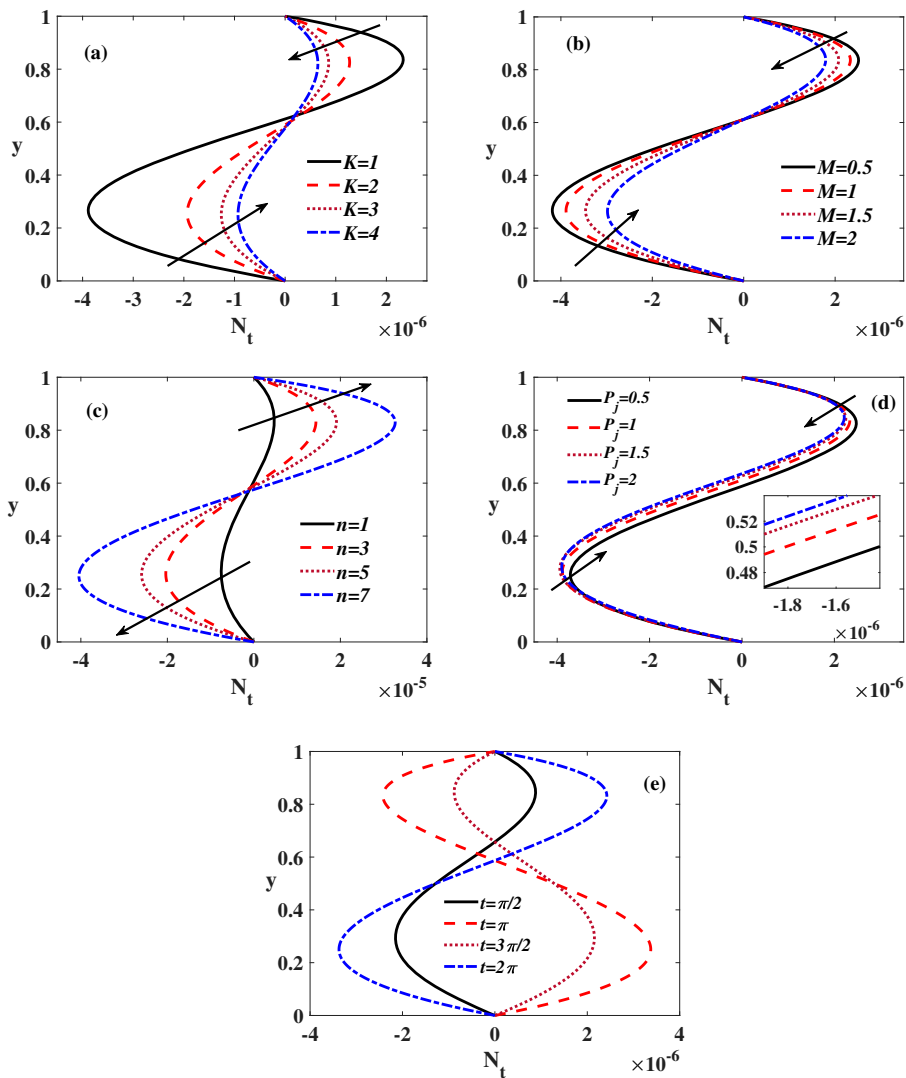


Figure 5. (a) Impact of K on N_t . (b) Impact of M on N_t . (c) Impact of n on N_t . (d) Impact of P_j on N_t . (e) Impact of t on N_t .

energy disparities. Increasing viscous dissipation increases the kinetic energy particle by decreasing the enthalpy factor, causing to enhance the temperature. Figure 6(b) displays that the steady temperature is diminished for given higher values in Hartmann number (M). Because the Lorentz forces slow down the flow movement which leads to decrease the temperature. Figure 6(c) shows that the steady temperature is decreasing due to rising values of the thermal relaxation time parameter δ . Because the particles of computable material have a greater chance of supplying heat to their adjacent particles when the relaxation time parameter of heat flux is increased, therefore energy is reduced. Figure 6(d) shows that the steady temperature is rising by varying the Brownian motion (Nb), because the random movement of nanoparticles creating friction to generate additional energy is the reason for

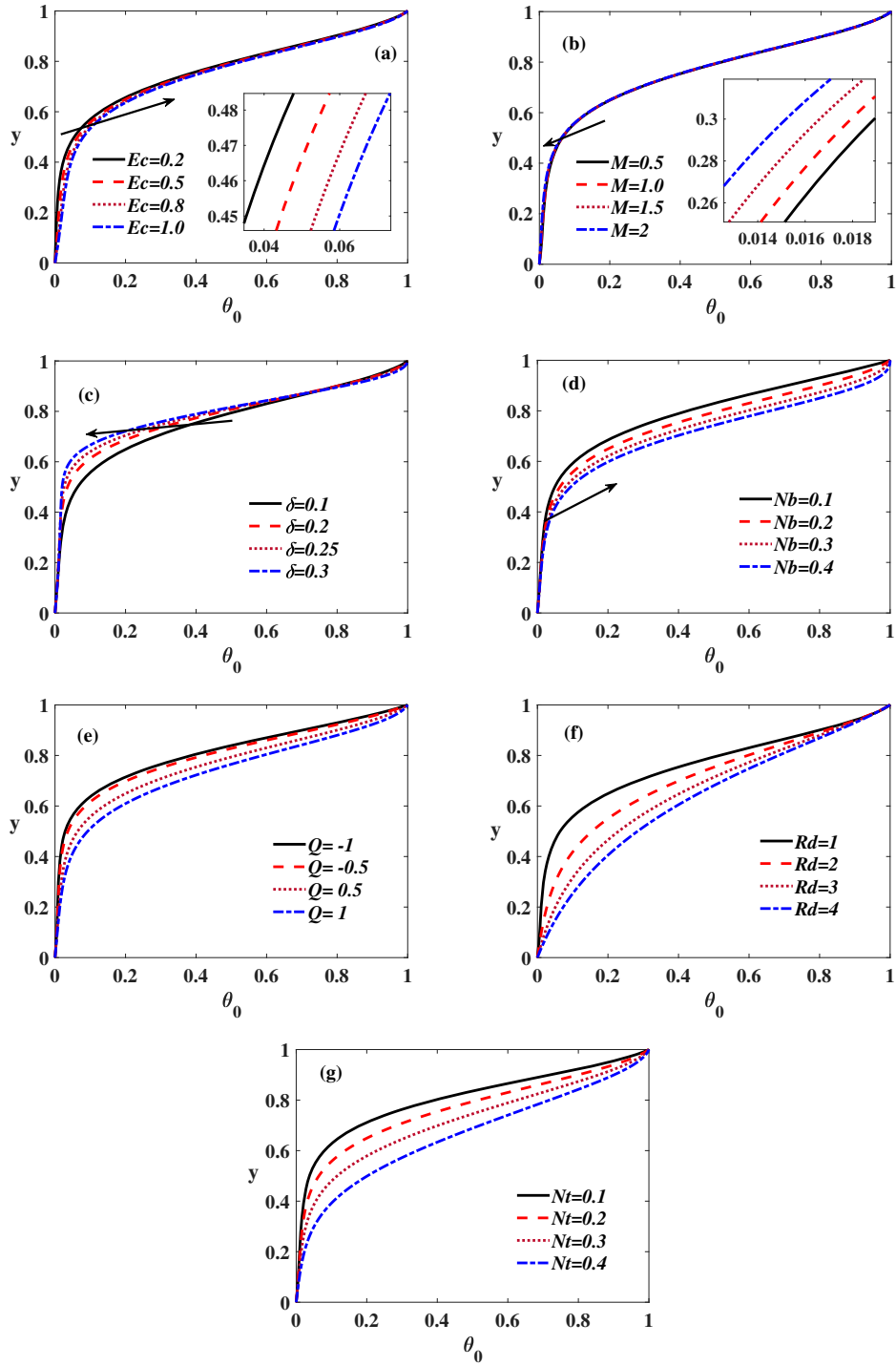


Figure 6. (a) Impact of Ec on θ_0 . (b) Impact of M on θ_0 . (c) Impact of δ on θ_0 . (d) Impact of Nb on θ_0 . (e) Impact of Q on θ_0 . (f) Impact of Rd on θ_0 . (g) Impact of Nt on θ_0 .

the rise the temperature. Figure 6(e) elucidates that the steady temperature is increasing by mounting the values for heat source ($Q > 0$) meanwhile diminishing over strengthening the heat sink ($Q < 0$). Figure 6(f) elucidates that the temperature is amplifying for the larger values of radiation parameter (Rd) which is the relative commitment of thermal radiation with the conductive heat of micropolar nanofluid and the same behavior occurs by varying the thermophoresis parameter (Nt) which is plotted in Figure 6(g).

Figure 7(a–h) describes the effects of Ec , M , δ , Nb , Nt , Rd , Q , and t on unsteady temperature distribution θ_t of micropolar nanofluid. Figure 7(a) and (b) portrays that the profiles of unsteady temperature are oscillating with an enhancement of the Eckert number (Ec) and Hartmann number (M). Figure 7(c) shows if the thermal relaxation time parameter (δ) is increased then the unsteady temperature is wavering on the walls. Figure 7(d) and (e) present the unsteady temperature oscillates with the boost up in the Brownian motion (Nb) and thermophoresis parameter (Nt). Figure 7(f) shows the variations of unsteady temperature due to giving distinct values for Rd . Figure 7(g) illustrates that the unsteady temperature is oscillating by mounting the values of the heat source ($Q > 0$) and heat sink ($Q < 0$). Figure 7(h) shows that the unsteady temperature is wavering due to giving distinct values for time (t).

Figure 8(a–f) portrays the steady nanoparticle concentration (ϕ_0) profiles for distinct values of Brownian motion parameter (Nb), Lewis number (Le), thermophoresis parameter (Nt), chemical reaction parameter (γ), and thermal relaxation time (δ). Figure 8(a) exhibits that the steady concentration is diminished with an enhancement of chemical reaction parameter. Subsequently, the steady concentration is reduced due to giving higher values in Lewis number presented in Figure 8(b). Figure 8(c) reveals that the steady concentration is diminished by giving higher values of thermal relaxation parameter. Even though particles of computable material have a greater chance of supplying heat to their adjacent particles as the relaxation time parameter of heat flux intensifies, the concentration decreases. Figure 8(d) demonstrates that the steady concentration is pulling up for an enhancement of the Brownian motion parameter. The reason behind this is active particles traveling over the wall in the fluid flow. Similarly, the opposite nature has happened in the rising of thermophoresis parameter which leads to the gradual improvement of the concentration of nanoparticles, and it is depicted in Figure 8(e).

The variations of γ , Le , δ , Nb , Nt , and t on the unsteady concentration (ϕ_t) of the micropolar nanofluid are given in Figure 9(a–f). Figure 9(a) and (b) illustrates that the unsteady concentration is wavering with the help of rising values of chemical reaction parameter (γ) and Lewis number (Le). Figure 9(c) presents the unsteady concentration fluctuating due to the increment of thermal relaxation parameter (δ). Figure 9(d) and (e) elucidates that the unsteady concentration is oscillates with the boosts up in the Brownian motion parameter (Nb) and thermophoresis parameter (Nt) accordingly. Figure 9(f) shows that the unsteady concentration is wavering between the walls for varying the values (t).

Figure 10(a–d) shows the variations of total entropy generation (NG) for various parameters Eckert number (Ec), Hartmann number (M), thermal radiation (Rd), and Brownian motion (Nb). Figure 10(a) displays that by increasing the Eckert number increases entropy generation due to internal friction acting on high fluid flow, followed by the collision of fluid molecules, which helps to increase entropy. Figure 10(b) depicts the entropy generation decelerates for rising the values of Hartmann number. Because drag forces are produced by the magnetic field and it causes to changes in entropy generation. From Figure 10(c),

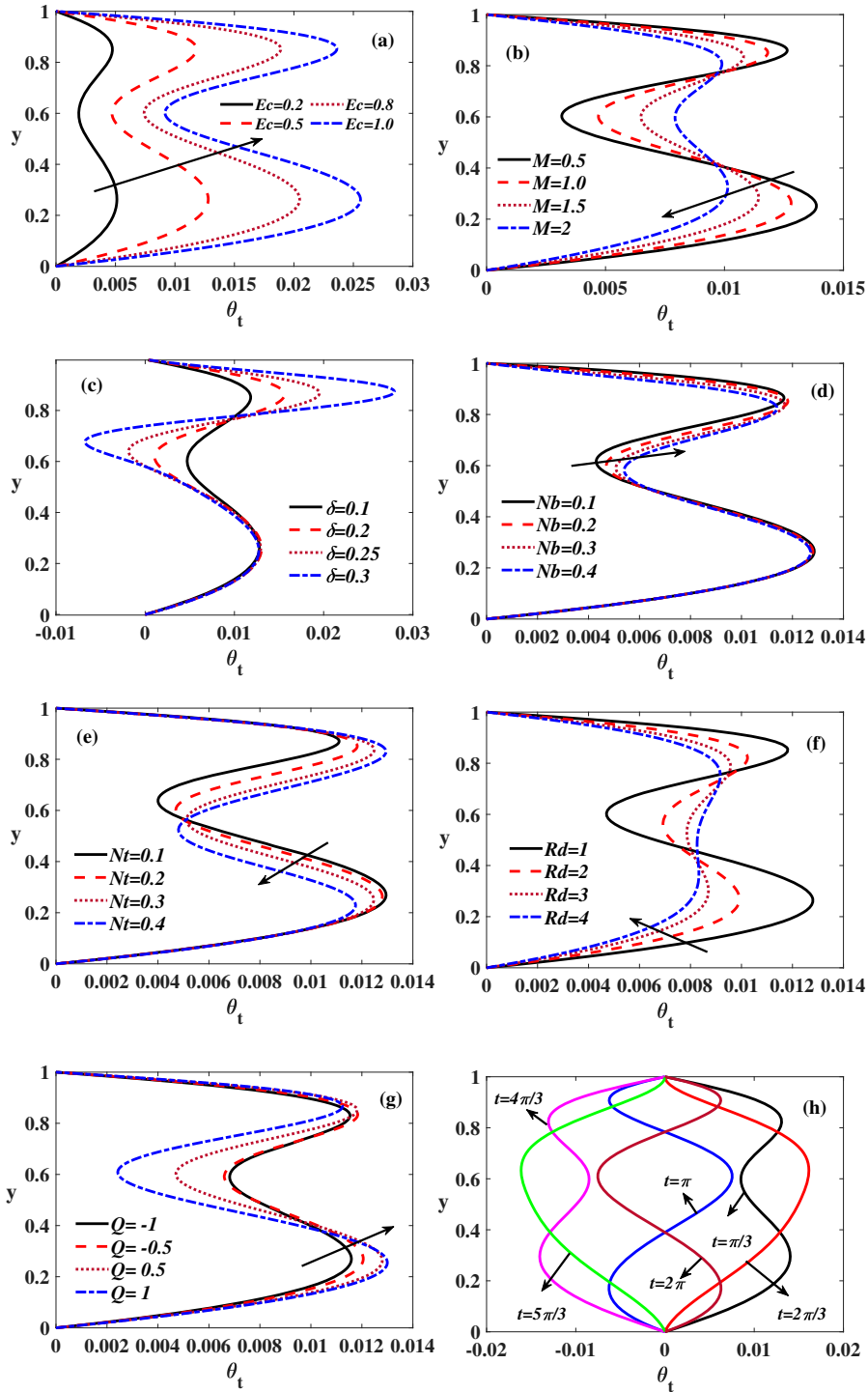


Figure 7. (a) Impact of E_c on θ_t . (b) Impact of M on θ_t . (c) Impact of δ on θ_t . (d) Impact of Nb on θ_t . (e) Impact of Nt on θ_t . (f) Impact of Rd on θ_t . (g) Impact of Q on θ_t . (h) Impact of t on θ_t .

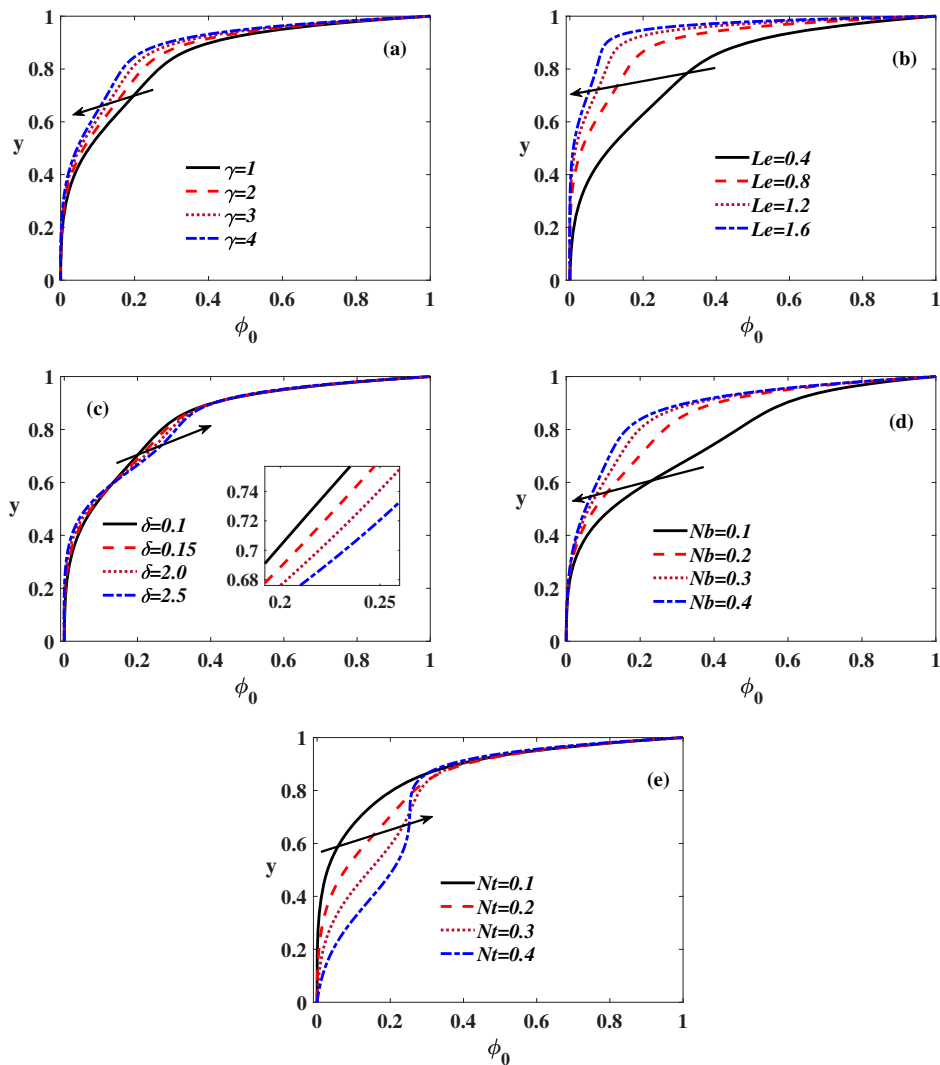


Figure 8. (a) Impact of γ on ϕ_0 . (b) Impact of Le on ϕ_0 . (c) Impact of δ on ϕ_0 . (d) Impact of Nb on ϕ_0 . (e) Impact of Nt on ϕ_0 .

it is noted that the variations of entropy are upsurged by giving higher values of thermal radiation, this is due to the thermal radiation's relative commitment with the conductive heat effects. Figure 10(d) illustrates that the magnitude of the entropy is amplifying at the center of the channel and it reduces close to the surface of top wall for escalating the values of Brownian motion.

The profiles of total Bejan number (Be) for the several parameters like Ec , M , Rd , Nb are incorporated in Figure 11(a–d). Figure 11(a) shows that the Bejan number is reduced in nature for larger values of Eckert number because dominating the impacts of fluid nonreversibility process in the walls. Figure 11(b) depicts the impacts of Hartmann number on Bejan number, it is found the increasing nature due to Lorentz acted on the flow and it leads to increase the Bejan number. Figure 11(c) is plotted the variations of Bejan for higher

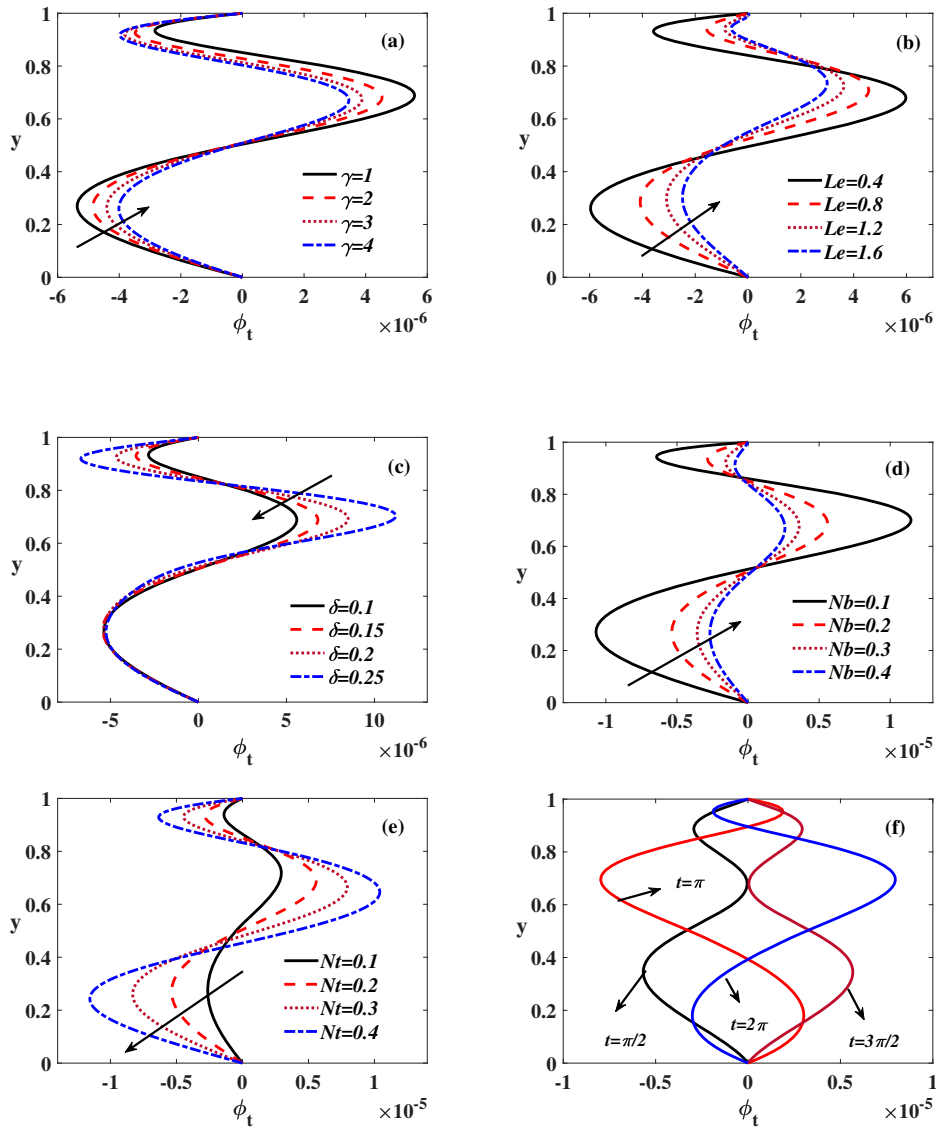


Figure 9. (a) Impact of γ on ϕ_t . (b) Impact of Le on ϕ_t . (c) Impact of δ on ϕ_t . (d) Impact of Nb on ϕ_t . (e) Impact of Nt on ϕ_t . (f) Impact of t on ϕ_t .

values of thermal radiation and it shows increasing behavior in both walls of the channel. Figure 11(d) exhibits the profiles of Bejan number for various values of Brownian motion parameter. Resulting that the enhancement in the lower wall, which is related to the heat irreversibility dominating close to the upper wall of the channel, therefore, the magnitude of Bejan number is decreased at the top wall in a channel.

The influences of steady velocity (u_0), unsteady velocity (u_t), steady microrotation (N_0), and unsteady microrotation (N_t) are presented numerically in Table 2 for various values of coupling parameter (K), Hartmann number (M), gyration parameter (n), and micro-inertia (n). The steady velocity is decreasing with the enhancement of coupling parameter and

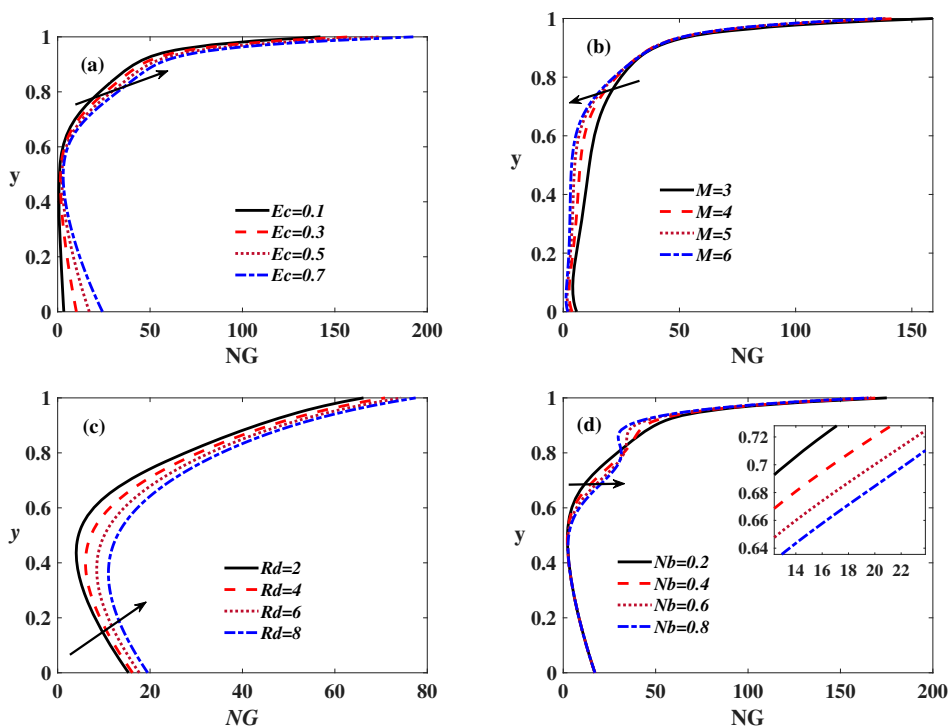


Figure 10. (a) Impact of Ec on NG . (b) Impact of M on NG . (c) Impact of Rd on NG . (d) Impact of Nb on NG .

Hartmann number while it is amplified by giving higher values of gyration parameter and micro-inertia. The steady microrotation is ascending with the increment of coupling parameter, and coupling parameter while it is descending with the enhancement of gyration parameter and micro-inertia. Similarly, the unsteady velocity and unsteady microrotation are wavering functions of K , M , n , and P_j .

The heat transfer rate (Nusselt number) and the mass transfer rate (Sherwood number) for steady and unsteady behavior at the lower wall for the different parameters M , Ec , K , Rd , Q , Nb , Nt , γ , Le , and δ are given in Table 3. In this table, the impacts at bottom wall for steady (Nu_0) and unsteady (Nu_t) Nusselt number are accelerated by boost up in Brownian motion, Eckert number, heat source/sink, thermophoresis parameter, and thermal relaxation parameter in the pulsating flow micropolar nanofluid, while they are diminished with an improvement of coupling parameter, Hartmann number, chemical reactive, and Lewis number.

The impacts of steady (Sh_0) and unsteady (Sh_t) mass transfer rate at the lower wall ($y = 0$) for various values of M , Ec , K , Rd , Q , Nb , Nt , γ , Le , and δ are presented, respectively. One can infer that the mass transfer rates for steady and unsteady are increased with the help of proceeding higher values of Hartmann number, coupling parameter, heat source/sink, thermal radiation, Brownian motion, and Lewis number. Similarly, the nature is inverted for an increment of Eckert number, thermophoresis, thermal relaxation, and chemical reactive parameter.

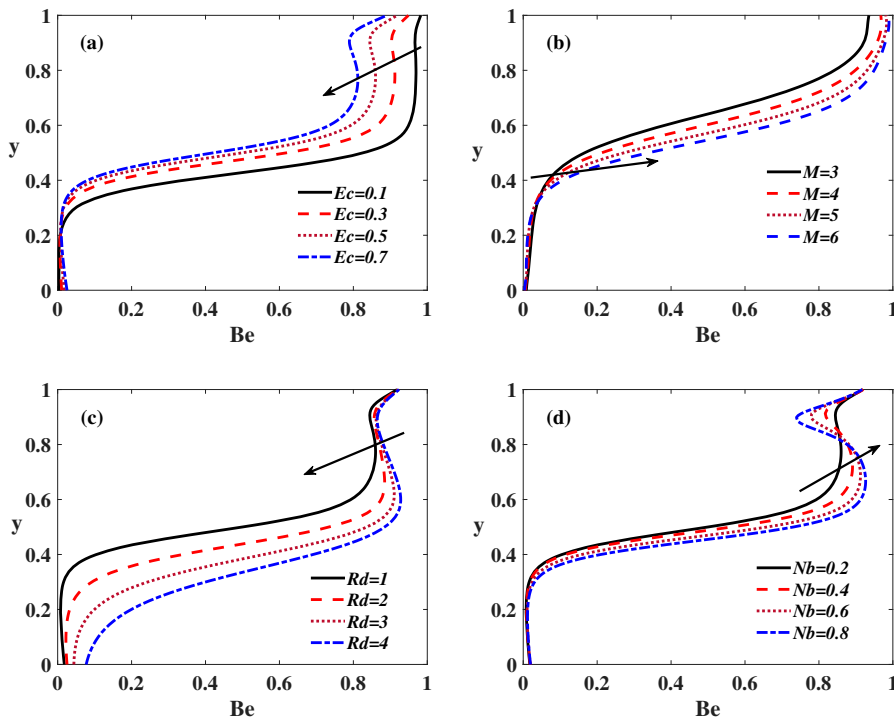


Figure 11. (a) Impact of Ec on Be . (b) Impact of M on Be . (c) Impact of Rd on Be . (d) Impact of Nb on Be .

5. Conclusions

The current work investigates the entropy generation of hydromagnetic pulsating flow of a micropolar nanofluid in a channel with the presence of Ohmic heating, viscous dissipation, Brownian motion, thermophoresis, and chemical reaction by employing the Buongiorno nanofluid model and the Cattaneo–Christov heat flux model. Here, micropolar fluid is picked as blood. Consciously, such work has some constraints which are beneficial in various fields such as biomedical, pharmaceuticals, nuclear reactors, electronics as well as biomedicine, and many industrial applications. In future, we can extend this model into emerging physical parameters with more efficient nanoparticles in the channel or plates. Presently, such work is essential in the investigation of cancer treatment, nano-drug delivery, human liver surgery with energy transport, polymer engineering, and biological fluid modeling. The obtained results for nondimensional fluid flow physical parameters are accomplished by using a shooting process via the Runge–Kutta fourth-order method. The influences of appropriate parameters like velocity, microrotation, temperature profiles, heat and mass transfer rate, entropy generation, and Bejan number of micropolar nanofluid are illustrated in detail by presenting graphical figures and tables. The key outcomes are summarized by the following.

- The velocity is diminished by amplifying the coupling parameter and Hartmann number.

Table 2. Steady and unsteady variations of velocity and microrotation (u_0, u_t, N_0, N_t) for K, M, n , and P_j when $\varepsilon = 0.1, t = \frac{\pi}{4}, Ec = 0.5, Pr = 21, K = 1, P_j = 1, n = 0.5, H = 2, \delta = 0.1, R = 1, Rd = 1, Q = 0.5, M = 1, Nb = 0.2, Nt = 0.2, \gamma = 1, Le = 1, Kr = 0.001, \lambda_0 = 1$, and $\lambda_1 = 1$.

y	Parameter	Values	u_0	u_t	N_0	N_t
0.3	K	1	0.088400924	0.007498289	-0.004314327	0.00749828
		2	0.048456904	0.003933707	-0.002141807	-0.00018841
		3	0.033282253	0.016115707	-0.001419433	0.032946309
0.6		1	0.111237678	0.009521362	-0.0002549272	-0.000019565
		2	0.058261907	0.004756969	0.0001291933	0.000871376
		3	0.039388845	0.018383780	0.0001489324	0.070071657
0.9		1	0.046518413	0.003917875	0.0022936441	0.000202909
		2	0.023016206	0.0018523212	0.0012664510	0.000107145
		3	0.015266590	0.0058725046	0.0008713764	0.089133562
0.3	M	0.5	0.094643868	0.008043761	-0.004668667	0.008043745
		1	0.088400943	0.007498289	-0.004314327	-0.000383556
		1.5	0.079675092	0.011219923	-0.00382166	0.01085688
0.6		0.5	0.119641018	0.010256322	-0.000289719	-0.000021002
		1	0.111237678	0.009521362	-0.000254927	-0.000019565
		1.5	0.099525998	0.011698888	-0.000207951	0.012275201
0.9		0.5	0.049696299	0.004195349	0.0024641722	0.000218386
		1	0.046518413	0.003917875	0.0022936441	0.000202909
		1.5	0.042084571	0.002434685	0.0020555861	-0.02590543
0.3	n	1	0.088845123	0.00753733	-0.008335620	0.007537339
		3	0.090623684	0.00769143	-0.022288831	-0.001990951
		5	0.092333104	0.02098394	-0.033891433	0.001348451
0.6		1	0.112193259	0.00960629	-0.000291117	-0.000022449
		3	0.115783679	0.00992314	0.000845387	0.000071873
		5	0.119039258	0.03001297	0.002926861	0.028602249
0.9		1	0.046757662	0.00393882	0.004627779	0.000408204
		3	0.047608142	0.004012968	0.014046935	0.001232157
		5	0.048343042	0.011580945	0.023232422	0.047664098
0.3	P_j	0.5	0.088458723	0.007502725	-0.004065500	0.007502725
		1	0.088400924	0.007498289	-0.004314327	-0.00038354
		1.5	0.088341504	0.008982411	-0.004503845	0.006380285
0.6		0.5	0.111253990	0.009522455	0.000248563	0.000018439
		1	0.111237678	0.009521362	-0.000254927	-0.000019565
		1.5	0.111211375	0.005398125	-0.000736654	-0.008841960
0.9		0.5	0.046500301	0.003916646	0.002413132	0.000208793
		1	0.046518413	0.003917875	0.002293644	0.000202909
		1.5	0.046533371	-0.003231504	0.002157515	-0.110189071

- The steady temperature is a rising function by mounting the thermal radiation, Brownian motion, thermophoresis parameter, and heat source.
- The steady concentration is diminished with an enhancement of Brownian motion, chemical reactive, and Lewis number.
- The entropy generation is accelerated by varying the values of viscous dissipation, thermal radiation, and Brownian motion.
- The Bejan number is dwindling for escalating values of Eckert number.
- Heat transfer rate is reduced with the boosts up in Hartmann number and coupling parameter while it is accelerating the thermal radiation and viscous dissipation.
- The steady and unsteady Sherwood numbers are reduced by increasing viscous dissipation, thermophoresis, and chemical reaction at the walls.

Table 3. Steady and unsteady variations of heat and mass transfer rates ($\theta'_0, \theta'_t, \phi'_0, \phi'_t$) for $M, Ec, K, Rd, Nb,$ and Nt when $\varepsilon = 0.1, t = \frac{\pi}{4}, Ec = 0.5, Pr = 21, K = 1, P_j = 1, n = 0.5, H = 2, \delta = 0.1, R = 1, Rd = 1, Q = 0.5 M = 1, Nb = 0.2, Nt = 0.2, \gamma = 1, Le = 1, Kr = 0.001, \lambda_0 = 1,$ and $\lambda_1 = 1$ at the wall ($y = 0$).

Parameter	Values	$(\theta'_0)_{y=0}$	$(\theta'_t)_{y=0}$	$(\phi'_0)_{y=0}$	$(\phi'_t)_{y=0}$
M	0.5	0.070849	0.010936	-0.002286	-0.003625
	1	0.063595	0.009797	-0.000172	-0.003204
	1.5	0.054129	0.008289	0.002520	-0.002649
	2	0.044584	0.006745	0.005134	-0.002086
Ec	0.1	0.014559	0.001946	0.009879	-0.000632
	0.3	0.039010	0.005858	0.004873	-0.001910
	0.5	0.063595	0.009797	-0.000172	-0.003204
	0.7	0.088317	0.013764	-0.005257	-0.004516
K	1	0.063595	0.009797	-0.000172	-0.003204
	2	0.040224	0.006210	0.003201	-0.002081
	3	0.029447	0.004423	0.005470	-0.001498
	4	0.023404	0.003417	0.006878	-0.001164
Rd	1	0.063595	0.009797	-0.000172	-0.003204
	2	0.100220	0.007920	0.038352	-0.002700
	3	0.186331	0.006712	0.066782	-0.002252
	4	0.280922	0.005938	0.078774	-0.001903
Q	-1	0.055855	0.009325	-0.011802	-0.003219
	-0.5	0.057808	0.009483	-0.009284	-0.003200
	0.5	0.063595	0.009797	-0.000172	-0.003204
	1	0.068775	0.009955	0.009349	-0.003244
Nb	0.1	0.062680	0.009793	-0.007213	-0.006383
	0.2	0.063595	0.009797	-0.000172	-0.003204
	0.3	0.064630	0.009802	0.002348	-0.002144
	0.4	0.065724	0.009807	0.003621	-0.001613
Nt	0.1	0.061621	0.009742	-0.003882	-0.001572
	0.2	0.063595	0.009797	-0.000172	-0.003204
	0.3	0.068784	0.009879	0.022217	-0.004985
	0.4	0.084076	0.010031	0.092957	-0.007180
γ	0.1	0.063595	0.009797	-0.000172	-0.003204
	0.2	0.063274	0.009795	-0.002840	-0.003051
	0.3	0.063061	0.009794	-0.004385	-0.002914
	0.4	0.063061	0.009794	-0.004385	-0.002914
Le	0.4	0.064313	0.009811	0.012917	-0.003770
	0.8	0.062693	0.009794	-0.006777	-0.002172
	1.2	0.062276	0.009799	-0.006074	-0.001489
	1.6	0.062085	0.009802	-0.005134	-0.001120
δ	0.1	0.063595	0.009797	-0.000172	-0.003204
	0.2	0.065058	0.010276	-0.008971	-0.003403
	0.25	0.067030	0.010438	-0.011190	-0.003499
	0.3	0.069215	0.010544	-0.012474	-0.003588

Disclosure statement

No potential conflict of interest was reported by the authors.

References

- [1] Choi SUS, Eastman J. Enhancing thermal conductivity of fluids with nanoparticles. Am Soc Mech Eng Fluids Eng Div. 1995;231:99–105.

- [2] Makinde OD, Animasaun IL. Thermophoresis and Brownian motion effects on MHD bioconvection of nanofluid with nonlinear thermal radiation and quartic chemical reaction past an upper horizontal surface of a paraboloid of revolution. *J Mol Liq.* 2016;221:733–743.
- [3] Zhang C, Zheng L, Zhang X, et al. MHD flow and radiation heat transfer of nanofluids in porous media with variable surface heat flux and chemical reaction. *Appl Math Model.* 2015;39:165–181.
- [4] Hussain Z, Hayat T, Alsaedi A, et al. Darcy Forchheimer aspects for CNTs nanofluid past a stretching cylinder; using Keller Box method. *Results Phys.* 2018;11:801–816.
- [5] Kumar A, Bhattacharyya K. Impacts of activation energy and binary chemical reaction on MHD flow of Williamson nanofluid in Darcy–Forchheimer porous medium. *Waves Random Complex Media.* 2021;31:1–22.
- [6] Buongiorno J. Convective transport in nanofluids. *J Heat Transf.* 2006;128:240–250.
- [7] Nield DA, Kuznetsov A V. Forced convection in a parallel-plate channel occupied by a nanofluid or a porous medium saturated by a nanofluid. *Int J Heat Mass Transf.* 2014;70:430–433.
- [8] Elelmy AF, Elgazery NS, Ellahi R. Blood flow of MHD non-Newtonian nanofluid with heat transfer and slip effects: application of bacterial growth in heart valve. *Int J Numer Methods Heat Fluid Flow.* 2020;30:4883–4908.
- [9] Ali B, Hussain S, Nie Y, et al. Finite element simulation of bioconvection and Cattaneo–Christov effects on micropolar based nanofluid flow over a vertically stretching sheet. *Chin J Phys.* 2020;68:654–670.
- [10] Afridi MI, Qasim M, Saleem S. Second law analysis of three dimensional dissipative flow of hybrid nanofluid. *J Nanofluids.* 2018;7:1272–1280.
- [11] Rajput S, Kumar A, Bhattacharyya K, et al. Unsteady nonlinear mixed convective flow of nanofluid over a wedge: Buongiorno model. *Waves Random Complex Media.* 2021;31:1–15.
- [12] Kumar CK, Srinivas S, Subramanyam Reddy A. MHD pulsating flow of Casson nanofluid in a vertical porous space with thermal radiation and Joule heating. *J Mech.* 2020;36:535–549.
- [13] Eringen A. Theory of micropolar fluids. *Indiana Univ Math J.* 1966;16:1–18.
- [14] Eringen AC. Theory of thermo-microstretch fluids and bubbly liquids. *Int J Eng Sci.* 1990;28:133–143.
- [15] Alzahrani F, Khan MI. Transportation of binary chemical reaction in entropy optimized micropolar fluid flow with activation energy and internal diffusion effects. *Waves Random Complex Media.* 2021;17:1–24.
- [16] Sheikholeslami M, Ganji D, et al. Heat and mass transfer of a micropolar fluid in a porous channel. *Commun Numer Anal.* 2014;2014:1–20.
- [17] Bitla P, Iyengar TKV. Pulsating flow of an incompressible micropolar fluid between permeable beds. *Nonlinear Anal Model Control.* 2013;18:399–411.
- [18] Hayat T, Javed M, Imtiaz M, et al. Convective flow of Jeffrey nanofluid due to two stretchable rotating disks. *J Mol Liq.* 2017;240:291–302.
- [19] Krishna MV, Chamkha AJ. Thermo-diffusion, chemical reaction, Hall and ion slip effects on MHD rotating flow of micro-polar fluid past an infinite vertical porous surface. *Int J Ambient Energy.* 2021;42:1–13.
- [20] Siddiq MK, Ashraf M. Bioconvection of micropolar nanofluid with modified Cattaneo–Christov theories. *Adv Mech Eng.* 2020;12:168781402092521.
- [21] Shah Z, Alzahrani EO, Dawar A, et al. Influence of Cattaneo–Christov model on Darcy–Forchheimer flow of micropolar ferrofluid over a stretching/shrinking sheet. *Int Commun Heat Mass Transf.* 2020;110:104385.
- [22] Ahmad S, Nadeem S, Muhammad N, et al. Cattaneo–Christov heat flux model for stagnation point flow of micropolar nanofluid toward a nonlinear stretching surface with slip effects. *J Therm Anal Calorim.* 2021;143:1187iEjEj1199.
- [23] Rajkumar D, Subramanyam Reddy A. Pulsating electrically conducting flow of Au/SWCNTs-blood micropolar nanofluid in a porous channel with Ohmic heating, thermal radiation. *Phys Scr.* 2021;96:125233.
- [24] Wang CY. Pulsatile flow in a porous channel. *J Appl Mech Trans ASME.* 1971;38:553–555.
- [25] Heat transfer to pulsatile flow in a channel. *Int J Heat Mass Transf.* 1977;20:171–173.
- [26] Bestman AR. Pulsatile flow in heated porous channel. *Int J Heat Mass Transf.* 1982;25:675–682.

- [27] Biswas S. Fundamental solution of steady oscillations in thermoelastic medium with voids. *Waves Random Complex Media*. 2020;30:1–17.
- [28] Bitla P, Iyengar TKV. Pulsating flow of an incompressible micropolar fluid between permeable beds with an inclined uniform magnetic field. *Eur J Mech B/Fluids*. 2014;48:174–182.
- [29] Srinivas S, Malathy T, Subramanyam Reddy A. A note on thermal-diffusion and chemical reaction effects on MHD pulsating flow in a porous channel with slip and convective boundary conditions. *J King Saud Univ – Eng Sci*. 2016;28:213–221.
- [30] Afridi MI, Qasim M. Second law analysis of Blasius flow with nonlinear Rosseland thermal radiation in the presence of viscous dissipation. *Propuls Power Res [Internet]*. 2019;8:234–242.
- [31] Abdelwahab AM, Mekheimer KS, Ali KK, et al. Numerical simulation of electroosmotic force on micropolar pulsatile bloodstream through aneurysm and stenosis of carotid. *Waves Random Complex Media*. 2021;31:1–32.
- [32] Srinivas S, Kumar CK, Reddy AS. Pulsating flow of Casson fluid in a porous channel with thermal radiation, chemical reaction and applied magnetic field. *Nonlinear Anal Model Control*. 2018;23:213–233.
- [33] Rajamani S, Subramanyam Reddy A. Pulsating flow of electrically conducting couple stress nanofluid in a channel with ohmic dissipation and thermal radiation-dynamics of blood. *Proc Inst Mech Eng Part E J Process Mech Eng*. 2021;235:779–784.
- [34] El Kot MA, Abd Elmaboud Y. Unsteady pulsatile fractional Maxwell viscoelastic blood flow with Cattaneo heat flux through a vertical stenosed artery with body acceleration. *J Therm Anal Calorim*. 2021;147:4355–4368.
- [35] Cattaneo C. On heat conduction. *Atti Sem Mat Fis Univ Modena*. 1948 [cited 8 Nov 2021]. p. 83–101.
- [36] Christov CI. On frame indifferent formulation of the Maxwell–Cattaneo model of finite-speed heat conduction. *Mech Res Commun*. 2009;36:481–486.
- [37] Dogonchi AS, Ganji DD. Impact of Cattaneo–Christov heat flux on MHD nanofluid flow and heat transfer between parallel plates considering thermal radiation effect. *J Taiwan Inst Chem Eng*. 2017;80:52–63.
- [38] Makinde OD, Sandeep N, Animasaun IL, et al. Numerical exploration of Cattaneo–Christov heat flux and mass transfer in magnetohydrodynamic flow over various geometries. *Defect Diffus Forum*. 2017;374:67–82.
- [39] Alebraheem J, Ramzan M. Flow of nanofluid with Cattaneo–Christov heat flux model. *Appl Nanosci*. 2020;10:2989–2999.
- [40] Jamshed W, Nisar KS, Ibrahim RW, et al. Computational frame work of Cattaneo–Christov heat flux effects on engine oil based Williamson hybrid nanofluids: a thermal case study. *Case Stud Therm Eng*. 2021;26:101179.
- [41] Yahya AU, Salamat N, Habib D, et al. Implication of bio-convection and Cattaneo–Christov heat flux on Williamson Sutterby nanofluid transportation caused by a stretching surface with convective boundary. *Chin J Phys*. 2021;73:706–718.
- [42] Garia R, Rawat SK, Kumar M, et al. Hybrid nanofluid flow over two different geometries with Cattaneo–Christov heat flux model and heat generation: a model with correlation coefficient and probable error. *Chin J Phys*. 2021;74:421–439.
- [43] Ghadikolaie SS, Hosseinzadeh K, Ganji DD, et al. Nonlinear thermal radiation effect on magneto Casson nanofluid flow with Joule heating effect over an inclined porous stretching sheet. *Case Stud Therm Eng*. 2018;12:176–187.
- [44] Fatunmbi EO, Salawu SO. Thermodynamic second law analysis of magneto-micropolar fluid flow past nonlinear porous media with non-uniform heat source. *Propuls Power Res*. 2020;9:281–288.
- [45] Venkatesan G. Joule heating impacts on MHD pulsating flow of Au/CuO-blood Oldroyd-B nanofluid in a porous channel. *Heat Transf*. 2021;50:7495–7513.
- [46] Lu D, Afridi MI, Allauddin U, et al. Entropy generation in a dissipative nanofluid flow under the influence of magnetic dissipation and transpiration. *Energies*. 2020;13:1–16.
- [47] Sharma BK, Sharma M, Gaur RK, et al. Mathematical modeling of magneto pulsatile blood flow through a porous medium with a heat source. *Int J Appl Mech Eng*. 2015;20:385–396.

- [48] Bhattacharyya A, Sharma R, Hussain SM, et al. A numerical and statistical approach to capture the flow characteristics of Maxwell hybrid nanofluid containing copper and graphene nanoparticles. *Chin J Phys.* 2021;77:1278–1290.
- [49] Srinivas S, Vijayalakshmi A, Subramanyam Reddy A, et al. MHD flow of a nanofluid in an expanding or contracting porous pipe with chemical reaction and heat source/sink. *Propuls Power Res.* 2016;5:134–148.
- [50] Abdal S, Siddique I, Alrowaili D, et al. Exploring the magnetohydrodynamic stretched flow of Williamson Maxwell nanofluid through porous matrix over a permeated sheet with bioconvection and activation energy. *Sci Rep [Internet].* 2022;12:1–12.
- [51] Venkatesan G, Reddy AS. Insight into the dynamics of blood conveying alumina nanoparticles subject to Lorentz force, viscous dissipation, thermal radiation, Joule heating, and heat source. *Eur Phys J Spec Top.* 2021;230:1475–1485.
- [52] Izadi M, Sheremet MA, Mehryan SAM, et al. MHD thermogravitational convection and thermal radiation of a micropolar nanofluid in a porous chamber. *Int Commun Heat Mass Transf.* 2020;110:104409.
- [53] Abbas MA, Ahmed B, Chen L, et al. Analysis of entropy generation on magnetohydrodynamic flow with mixed convection through porous media. *Energies.* 2022;15:1–20.
- [54] Hayat T, Qayyum S, Alsaedi A, et al. Radiation effects on the mixed convection flow induced by an inclined stretching cylinder with non-uniform heat source/sink. *PLoS ONE.* 2017;12:1–23.
- [55] Nadeem S, Ijaz M, Ayub M. Darcy–Forchheimer flow under rotating disk and entropy generation with thermal radiation and heat source/sink. *J Therm Anal Calorim.* 2021;143:2313–2328.
- [56] Bejan A. A study of entropy generation in fundamental convective heat V-. *J Heat Transf.* 1979;101:718–725.
- [57] Afridi MI, Qasim M, Saleem S. Second law analysis of three dimensional dissipative flow of hybrid nanofluid. *J Nanofluids.* 2018;7:1272–1280.
- [58] Roja A, Gireesha BJ, Prasannakumara BC. MHD micropolar nanofluid flow through an inclined channel with entropy generation subjected to radiative heat flux, viscous dissipation and multiple slip effects. *Multidiscip Model Mater Struct.* 2020;16:1475–1496.
- [59] Lu D, Afridi MI, Allauddin U, et al. Entropy generation in a dissipative nanofluid flow under the influence of magnetic dissipation and transpiration. *Energies.* 2020;13:1–16.
- [60] Afridi MI, Qasim M, Khan NA, et al. Minimization of entropy generation in MHD mixed convection flow with energy dissipation and Joule heating: utilization of Sparrow–Quack–Boerner local non-similarity method. *Defect Diffus Forum.* 2018;387:63–77.
- [61] Almakki M, Mondal H, Sibanda P. Onset of unsteady MHD micropolar nanofluid flow with entropy generation. *Int J Ambient Energy.* 2021;42:1–4.
- [62] Ijaz Khan M, Alzahrani F. Numerical simulation for the mixed convective flow of non-Newtonian fluid with activation energy and entropy generation. *Math Methods Appl Sci.* 2021;44:7766–7777.
- [63] Afridi MI, Qasim M, Wakif A, et al. Second law analysis of dissipative nanofluid flow over a curved surface in the presence of Lorentz force: utilization of the Chebyshev–Gauss–Lobatto spectral method. *Nanomaterials.* 2019;9:195.